

Nonlinear mechanics with photonic crystal nanomembranes

Thomas Antoni,^{1,2,*} Kevin Makles,¹ Rémy Braive,^{2,3} Tristan Briant,¹ Pierre-François Cohadon,¹ Isabelle Sagnes,² Isabelle Robert-Philip,² and Antoine Heidmann¹

¹Laboratoire Kastler Brossel, UPMC-ENS-CNRS, Case 74,
4 place Jussieu, F75252 Paris Cedex 05, France

²Laboratoire de Photonique et de Nanostructures LPN-CNRS,
UPR-20, Route de Nozay, 91460 Marcoussis, France

³Université Paris Diderot, 75205 Paris, Cedex 13, France

Optomechanical systems close to their quantum ground state (QGS) [1, 2] and nonlinear nanoelectromechanical systems (NEMS) are two hot topics of current physics research. Demonstrating the QGS allows to shed new light on quantum coherent effects in meso- and macroscopic systems, whereas NEMS operated in a nonlinear regime [3] are used either to demonstrate the underlying physics of sheer nonlinear effects [4–6] or as RF amplifiers, with sensitivity improvement both at the classical [7, 8] or quantum noise level [9, 10]. As high-reflectivity and low mass are crucial features to improve optomechanical coupling towards the QGS, we have designed, fabricated and characterized photonic crystal (PhC) nanomembranes [11], at the crossroad of both topics. Here we demonstrate a number of nonlinear effects with these membranes. We first characterize the nonlinear behavior of a single mechanical mode and we demonstrate its nonlocal character by monitoring the subsequent actuation-related frequency shift of a different mode. We then proceed to study the underlying nonlinear dynamics, both by monitoring the phase-space trajectory of the free resonator and by characterizing the mechanical response in presence of a strong pump excitation. We observe in particular the frequency evolution during a ring-down oscillation decay, and the emergence of a phase conjugate mechanical response to a weaker probe actuation. Our results are crucial to understand the full nonlinear features of the PhC membranes, and possibly to look for nonlinear signatures of the quantum dynamics [12].

We focus on the mechanical nonlinear behavior of photonic crystal nanomembranes developed as end mirrors in a Fabry-Perot optomechanical cavity [11]. Details about the mechanical and optical properties, as well as the fabrication process of these membranes are described in previous publications [11, 13, 14]. They are $10\ \mu\text{m} \times 20\ \mu\text{m} \times 260\ \text{nm}$ indium phosphide slabs suspended over the substrate by four decoupling bridges ($0.5\text{-}\mu\text{m}$ width and 6- to $12\text{-}\mu\text{m}$ lengths) located at the nodes of the mechanical mode of interest [15], $5.9\ \mu\text{m}$ away from the center of the membrane.

To probe the mechanical response of the membrane, the sample is actuated by a piezoelectric stack, and the membrane displacement is monitored by a Michelson interferometer (see Fig. 1). The sample is operated in a vacuum chamber at 10^{-2} mbar to prevent from air viscous damping and squeezed film effects. We use three different membranes with resonance frequencies $\Omega_0/2\pi = 782\ \text{kHz}$, $1036\ \text{kHz}$, and $1057\ \text{kHz}$, and quality factors $Q \simeq 5000$, mainly limited by surface effects.

A network analyzer actuates the sample and monitors the resulting displacement spectrum. Figure 2 (left) shows the forced oscillation amplitude $\tilde{x}_p[\Omega_p]$ as a function of the actuation frequency Ω_p , for different actuation powers. The mode of interest, close to 1 MHz for the membrane used here, exhibits a strong nonlinearity even for an actuation voltage limited to a few volts applied to the piezoelectric stack, corresponding to displacements of a few picometers only for the substrate and at the nanometric level for the membrane.

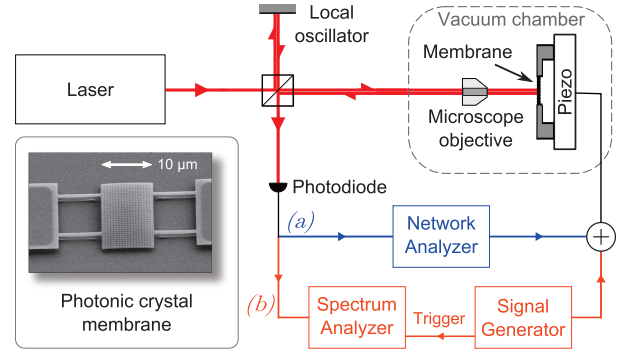


FIG. 1. Interferometric setup: we use either a network analyzer to probe the mechanical response of the membrane (a), or a signal generator and a spectrum analyzer triggered by the generator to test the ring-down behavior (b), or both of them to perform pump-probe experiments. The inset shows a typical photonic crystal membrane.

The nonlinearity can be accounted for by the Duffing model in which the resonance frequency has a quadratic dependence with the displacement $x_p(t)$:

$$\ddot{x}_p(t) + \Gamma \dot{x}_p(t) + \Omega_0^2 [1 + \beta x_p^2(t)] x_p(t) = \alpha_p(t), \quad (1)$$

where $\alpha_p(t) = 2\tilde{\alpha}_p \cos(\Omega_p t)$ is the driving force, $\Gamma = \Omega_0/Q$ the mechanical damping, and β the nonlinearity strength.

At first order the forced displacement is mainly monochromatic at the actuation frequency Ω_p , with a

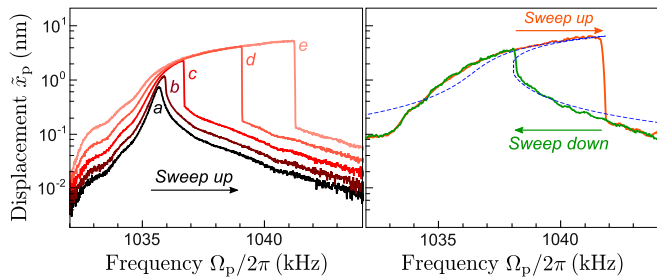


FIG. 2. Oscillation amplitude $\tilde{x}_p[\Omega_p]$ of the membrane as a function of the piezoelectric actuation frequency Ω_p . Linear to nonlinear transition is clearly visible on left curves *a* to *e*, obtained with an upward frequency sweep of the network analyzer and for increasing actuation powers (10 dBm to 30 dBm with a 5-dB step). Curves on the right are swept either up or down with the frequency generator at 30 dBm and exhibit a typical hysteresis cycle as expected from the theoretical fit (dashed curve).

Fourier component given by (assuming $Q \gg 1$)

$$\tilde{x}_p[\Omega_p] = \frac{\tilde{\alpha}_p}{\Omega_0^2 (1 + \varepsilon) - \Omega_p^2 - i\Gamma\Omega_0}. \quad (2)$$

This expression corresponds to the usual Lorentzian resonance, except for a shift of the resonance frequency proportional to the mean square displacement through the term

$$\varepsilon = 3\beta |\tilde{x}_p[\Omega_p]|^2. \quad (3)$$

This shift is responsible for the spectra observed in Fig. 2, as shown by the theoretical fit on the right (dashed curve). Although higher order effects must be considered to completely fit the displacement, values of β can nonetheless be evaluated in the range of 10^{13} m^{-2} . Also note that such a more complete derivation [16] would lead to the emergence of odd harmonics of motion with an amplitude at least $\varepsilon \lesssim 10^{-3}$ times smaller than the fundamental oscillation at Ω_p .

Stable solutions of eqs. (2) and (3) correspond to the upper and lower branches of a bistable hysteresis cycle. As the network analyzer only sweeps frequencies upward, curves in Fig. 2 (left) explore the upper branch until they suddenly fall down to the lower branch. To sweep frequency either up or down, we make use of a signal generator together with a spectrum analyzer in max-hold configuration (see setup *b* in Fig. 1). Both sweeps are shown in Fig. 2 (right) and clearly exhibits an hysteresis cycle.

The nonlinearity arises from additional stress induced by large displacements and we expect nonlocal effects as intrinsic elastic parameters such as Young's modulus of the membrane may be affected [17, 18]. We have thus investigated the influence of one mode (mode 1) on the natural frequency of another one (mode 2), using both

the signal generator and the network analyzer as shown in Fig. 1.

An upward frequency sweep is first produced by the signal generator with a 20-dBm power to actuate the first mode in its nonlinear regime. In order to explore different points on the upper branch of the nonlinearity, the sweep is stopped at different frequencies Ω_p , represented by the arrows in Fig. 3 (left). While the drive of mode 1 remains at that frequency, we monitor the linear response of mode 2 using the network analyzer with a 0-dBm actuation power. Central curves in Fig. 3, obtained for increasing actuation frequencies Ω_p , clearly show that the resonance frequency Ω_s of mode 2 is shifted as the displacement amplitude of mode 1 gets larger and larger. Considering that mode 2 has a quality factor of 6000, the mode is actually displaced 170 times its width. We also explore the lower branch of the nonlinear response of mode 1 using an initial downward frequency sweep (Fig. 3 right), thus retrieving the bistable behavior of mode 1 on the resonance-frequency shift of mode 2.

As the effective elastic parameters of the membrane are altered by the nonlinearity, one may also expect a modification of its dynamics, which we have investigated using a ring-down technique. We have thus monitored the motion of the membrane in phase space, defining the slowly varying quadratures X_1 and X_2 as:

$$x_p(t) = X_1(t) \cos(\Omega_0 t) + X_2(t) \sin(\Omega_0 t). \quad (4)$$

X_1 and X_2 are readily accessible using the spectrum analyzer in IQ demodulation mode. Figure 4 shows the forced regime and the ring-down decay of the mechanical mode for different actuation levels: in the linear regime at its natural frequency Ω_0 (left column), in the linear regime out of resonance (central column), and in the nonlinear regime (right column). The membrane is actuated for times $t < 0$, with an upward frequency sweep to get the mode on the upper branch in the nonlinear case, then

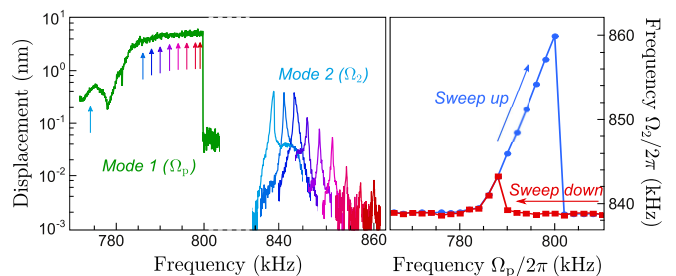


FIG. 3. Intermodal coupling: actuation of mode 1 in its nonlinear regime (left curve) induces a frequency shift of the resonance of mode 2 (central curves) when the actuation frequency Ω_p of mode 1 is increased along the upper branch (arrows). Right curves display the bistable behavior of the resonance frequency Ω_s of mode 2 when Ω_p is either swept up or down. The nonlinearity strength of mode 1 is comparable to the one experienced in curve *e* in Fig. 2.

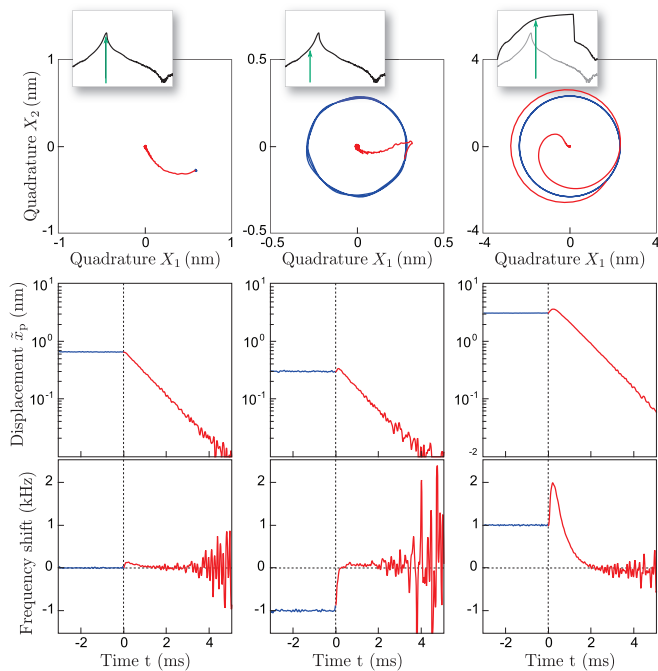


FIG. 4. Time evolution in phase-space for the forced (blue) and free (red) regimes. Three cases are investigated, as sketched on top of each column, from left to right: linear regime actuated at resonance (5 dBm at 1057 kHz), out of resonance (9 dBm at 1056 kHz), and nonlinear regime (29 dBm at 1058 kHz). Curves from top to bottom represent the phase-space trajectories and the amplitude and frequency evolutions.

the actuation is stopped by a fast switch at time $t = 0$.

The phase-space trajectories (top curves) first show the forced regime which appears as blue circles or as a single stationary point in the resonant case (left), and second the ring-down regime displayed as red spirals which reduce to an almost straight line down to the origin when the motion is close to resonance.

From these data we can infer the time evolutions of both the amplitude and frequency of motion (middle and bottom curves). In contrast to other systems such as graphene [19], the amplitude decay time is the same in the different actuation regimes: $\tau = 1/\Gamma \simeq 0.56$ ms, corresponding to a mechanical quality factor $Q \simeq 3700$. This tends to confirm that the damping in these resonators does not depend on the effective Young modulus and is indeed mostly due to surface effects [11].

Yet the frequency behavior drastically changes between the linear and nonlinear regimes. In the former case, even for a non-resonant actuation, the frequency instantaneously jumps back to its natural value when the actuation is released, as can also be inferred from the straight line trajectories in phase space. This result is actually expected for a linear harmonic oscillator, as its free evolution for $t > 0$ only depends on the initial position and speed at $t = 0$, and not on the previous forced

actuation frequency. In the nonlinear case, the frequency hops towards the top of the upper bistability branch and then slowly relaxes down to the natural frequency as the nonlinearity fades out. This can be understood from eq. (2) which shows that for a given oscillation amplitude \tilde{x}_p , the preferred oscillation frequency is $\Omega_0(1 + \varepsilon/2)$ [16]. As the oscillation amplitude and then the nonlinear coefficient ε [eq. (3)] exponentially decrease with time, one thus expects the same behavior for the free oscillation frequency.

To confirm this interpretation, we have studied the mechanical response of the mode to a weak probe excitation while it is simultaneously set in the nonlinear regime by a strong pump actuation. The setup is actually similar to the one used for the two-mode actuation (Fig. 3), except that both pump and probe are actuating the same mechanical mode, close to its natural frequency $\Omega_0/2\pi \simeq 782$ kHz for the membrane used here. Figure 5 (left) shows the spectra $\tilde{x}_s[\Omega_s]$ obtained when the probe frequency Ω_s is scanned around the pump frequency Ω_p , for different pump actuation powers. We clearly observe two symmetrical lorentzian peaks whose frequency difference increases with the pump power.

Using a spectrum analyzer instead of a network analyzer, we actually checked that the two resonances *simultaneously* appear: when actuated at a frequency Ω_s , the pump-probe combination leads to the concomitant generation of a mechanical response at frequencies Ω_s and $2\Omega_p - \Omega_s$, symmetrically disposed on both sides of the pump frequency.

This behavior can be understood from the Duffing equation (1), adding a second source term $\alpha_s(t) = 2\tilde{\alpha}_s \cos(\Omega_s t)$ related to the probe. The cubic term in Duffing equation is then responsible for the mixing of pump and probe signals, in a way similar to a $\chi^{(3)}$ nonlinearity in optics. Indeed, writing the total displacement in presence of the probe as the sum of the unperturbed

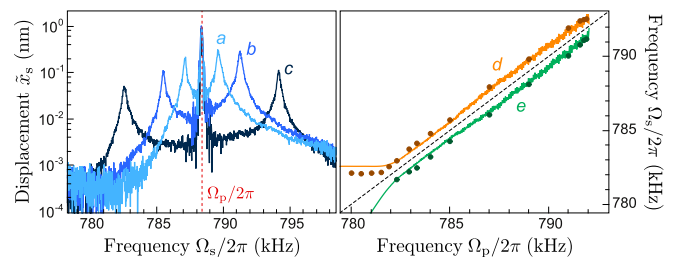


FIG. 5. Mechanical response of a mode pumped in the nonlinear regime (frequency Ω_p) and probed by a weak actuation (frequency Ω_s). Spectra obtained with pump actuation powers of 10, 20, and 30 dBm (curves *a* to *c*) exhibit two resonances symmetrically disposed around the pump frequency Ω_p , as demonstrated by curves *d* and *e*: dots are experimental values of the two resonance frequencies obtained for a pump actuation of 5 dBm (leading to a nonlinearity strength similar to curve *c* in Fig. 2), solid curves are theoretical fits.

displacement $x_p(t)$ due to the pump only [eq. (2)] and an additional displacement $x_s(t)$, we obtain the following equation (assuming $|\tilde{x}_s| \ll |\tilde{x}_p|$):

$$\ddot{x}_s(t) + \Gamma \dot{x}_s(t) + \Omega_0^2 [1 + 3\beta x_p^2(t)] x_s(t) = \alpha_s(t). \quad (5)$$

As $x_p(t)$ is oscillating at frequency Ω_p , the nonlinear term $x_p^2(t)$ contains both a static term and a fast oscillation at $2\Omega_p$. The former is responsible for a modification of the linear mechanical response at frequency Ω_s whereas the latter is formally similar to phase conjugation in optics and generates a response at $2\Omega_p - \Omega_s$. From (5) one gets the following coupled equations for the two Fourier components of x_s at frequencies Ω_s and $2\Omega_p - \Omega_s$:

$$\zeta[\Omega_s] \tilde{x}_s[\Omega_s] + \varepsilon \Omega_0^2 \tilde{x}_s^*[2\Omega_p - \Omega_s] = \tilde{\alpha}_s, \quad (6)$$

$$\zeta[2\Omega_p - \Omega_s] \tilde{x}_s^*[2\Omega_p - \Omega_s] + \varepsilon \Omega_0^2 \tilde{x}_s[\Omega_s] = 0, \quad (7)$$

where $\zeta[\Omega] = \Omega_0^2(1 + 2\varepsilon) - \Omega^2 - i\Gamma\Omega_0$, and we have assumed for simplicity \tilde{x}_p real. We thus obtain two phase-conjugate lorentzian responses with resonance frequencies:

$$\Omega_{s+} = \Omega_0(1 + \varepsilon), \quad \Omega_{s-} = 2\Omega_p - \Omega_{s+}. \quad (8)$$

Note the difference between Ω_{s+} and the resonance frequency $\Omega_0(1 + \varepsilon/2)$ in response to a single actuation [eq. (2)], actually equivalent to the difference obtained between self- and cross-phase modulations in Kerr media[20].

Dots in Fig. 5 (right) show frequencies Ω_{s+} and Ω_{s-} deduced from spectra similar to the ones displayed on Fig. 5 (left), as a function of the pump frequency Ω_p . Curves *d* and *e* are theoretical predictions obtained using eqs. (8) with ε estimated from the experimental nonlinear behavior [eq. (2) and Fig. 2]. At low pump frequency $\Omega_p \lesssim \Omega_0$, the membrane is almost in a linear regime and we only observe one peak close to the natural frequency Ω_0 . At higher frequency, the two resonances are symmetrically located around Ω_p (dashed line), in good agreement with theoretical predictions.

We have demonstrated nonlinear effects in the dynamics of PhC nanomembranes: bistability, intermodal tuning and the generation of phase conjugate modes. Pump-probe experiments have in particular allowed us to underline the non-local character of the Young modulus modification. Such nonlinear behaviours are intrinsic to nano- and microscale systems[3], and have dramatic consequences not only in the fields of optomechanics and nonlinear dynamics, but in quantum optics as well, as intermodal coupling can be used to perform QND measurements of a signal mode by monitoring a meter one [21–23]. Optomechanical systems can also be used for classical or quantum information processing, either by taking advantage of their long mechanical coherence times to store information in a mechanical excitation [24], or by using their nonlinear character for non volatile memories [25].

* thomas.antonis@spectro.jussieu.fr

- [1] Teufel, J. D. et al. Sideband cooling of micromechanical motion to the quantum ground state. *Nature* **475**(7356), 359 (2011).
- [2] Chan, J. et al. Laser cooling of a nanomechanical oscillator into its quantum ground state. *Nature* **478**(7369), 89 (2011).
- [3] Rhoads, J. F., Shaw, S. W., and Turner, K. L. Nonlinear dynamics and its applications in micro- and nanoresonators. *J. Dyn. Syst.-T. ASME*. **132**(3), 034001 (2010).
- [4] Aldridge, J. S. and Cleland, A. N. Noise-enabled precision measurements of a Duffing nanomechanical resonator. *Phys. Rev. Lett.* **94**, 156403, Apr (2005).
- [5] Kozinsky, I., Postma, H. W. C., Kogan, O., Husain, A., and Roukes, M. L. Basins of attraction of a nonlinear nanomechanical resonator. *Phys. Rev. Lett.* **99**, 207201, Nov (2007).
- [6] Unterreithmeier, Q. P., Faust, T., and Kotthaus, J. P. Nonlinear switching dynamics in a nanomechanical resonator. *Phys. Rev. B* **81**, 241405, Jun (2010).
- [7] Almog, R., Zaitsev, S., Shtempluck, O., and Buks, E. High intermodulation gain in a micromechanical Duffing resonator. *Appl. Phys. Lett.* **88**(21), 213509 (2006).
- [8] Defoort, M. et al. Audio mixing in a tri-port nanoelectro-mechanical device. *Appl. Phys. Lett.* **99**(23), 233107 (2011).
- [9] Almog, R., Zaitsev, S., Shtempluck, O., and Buks, E. Noise squeezing in a nanomechanical Duffing resonator. *Phys. Rev. Lett.* **98**, 078103, Feb (2007).
- [10] Mahboob, I., Wilmart, Q., Nishiguchi, K., Fujiwara, A., and Yamaguchi, H. Wide-band idler generation in a GaAs electromechanical resonator. *Phys. Rev. B* **84**, 113411, Sep (2011).
- [11] Antoni, T. et al. Deformable two-dimensional photonic crystal slab for cavity optomechanics. *Opt. Lett.* **36**(17), 3434–3436 (2011).
- [12] Katz, I., Retzker, A., Straub, R., and Lifshitz, R. Signatures for a classical to quantum transition of a driven nonlinear nanomechanical resonator. *Phys. Rev. Lett.* **99**, 040404, Jul (2007).
- [13] Gavartin, E. et al. Optomechanical coupling in a two-dimensional photonic crystal defect cavity. *Phys. Rev. Lett.* **106**(20), 203902 (2011).
- [14] Talneau, A., Lee, K. H., Guilet, S., and Sagnes, I. Efficient coupling to W1 photonic crystal waveguide on InP membrane through suspended access guides. *Appl. Phys. Lett.* **92**(6), 061105 (2008).
- [15] Cole, G. D., Wilson-Rae, I., Werbach, K., Vanner, M. R., and Aspelmeyer, M. Phonon-tunnelling dissipation in mechanical resonators. *Nat. Commun.* **2**, 231 (2011).
- [16] Landau, L. D. and Lifshitz, E. M. *Mechanics, Course of theoretical physics, vol. 1, 3rd edition* (Butterworth-Heinemann, Oxford, 1976).
- [17] Westra, H. J. R. et al. Interactions between directly- and parametrically-driven vibration modes in a micromechanical resonator. *Phys. Rev. B* **84**, 134305 (2011).
- [18] Venstra, W. J., Westra, H. J. R., and van der Zant, H. S. J. Q-factor control of a microcantilever by mechanical sideband excitation. *Appl. Phys. Lett.* **99**(15), 151904 (2011).
- [19] Eichler, A. et al. Nonlinear damping in mechanical res-

- onators made from carbon nanotubes and graphene. *Nat. Nano.* **6**(6), 339 – 342 (2011).
- [20] Agrawal, G. P., *Nonlinear Fiber Optics* (Academic Press, Boston, 1989).
- [21] Grangier, P., Levenson, J. A., and Poizat, J.-P. Quantum non-demolition measurements in optics. *Nature* **396**(6711), 537 (1998).
- [22] Westra, H. J. R., Poot, M., van der Zant, H. S. J., and Venstra, W. J. Nonlinear modal interactions in clamped-clamped mechanical resonators. *Phys. Rev. Lett.* **105**(11), 117205 (2010).
- [23] Santamore, D. H., Doherty, A. C., and Cross, M. C. Quantum nondemolition measurement of Fock states of mesoscopic mechanical oscillators. *Phys. Rev. B* **70**, 144301 (2004)
- [24] Weis, S. et al. Optomechanically Induced Transparency. *Science* **330**, 1520 (2010).
- [25] Bagheri, M., Poot, M., Li, M., Pernice, W. P. H., and Tang, H. X. Dynamic manipulation of nanomechanical resonators in the high-amplitude regime and non-volatile mechanical memory operation. *Nat. Nano.* **6**, 726 (2011).